thalassemia reports

MDPI

Article

Comparative Diagnostic Value of 3D Volumetry and Speckle-Tracking over Conventional 2D Echocardiography in the Evaluation of Left Ventricular Function in Pediatric Transfusion-Dependent Beta-Thalassemia

Omar Raafat [1,*], Ahmed Salama Abouhay [1], Yasmine El Chazli [2], Yasser Wali [3] and Hani Mahmoud Adel [1]

[1] Pediatric Cardiology Unit, Department of Pediatrics, Faculty of Medicine, Alexandria University, Alexandria 21526, Egypt; ahmedabuhy1750@gmail.com (A.S.A.); haniadel70@hotmail.com (H.M.A.)
[2] Pediatric Hematology Unit, Department of Pediatrics, Faculty of Medicine, Alexandria University, Alexandria 21526, Egypt; yasmine.chazli@alexmed.edu.eg
[3] Department of Child Health, College of Medicine and Health Sciences, Sultan Qaboos University, Muscat 123, Oman; yasser_wali@hotmail.com
* Correspondence: o_riad16@alexmed.edu.eg

Abstract

Background: Left ventricular (LV) dysfunction remains the leading cause of mortality in transfusion-dependent beta-thalassemia (TDßT), yet conventional echocardiography often fails to detect early myocardial impairment. This study aimed to comprehensively evaluate LV function in children with TDßT using three-dimensional echocardiography (3DE) and speckle-tracking strain analysis, comparing diagnostic performance with conventional two-dimensional (2D) parameters. **Results:** 50 TDßT patients were compared to 50 matched controls and exhibited preserved conventional LV ejection fraction (EF) on 2D (65.31 ± 7.12% vs. 69.21 ± 3.87%, $p = 0.001$), but 3DE revealed significant ventricular dilation with higher end-diastolic volume index (75.50 ± 17.99 vs. 65.63 ± 11.86 mL/m^2, $p = 0.002$) and end-systolic volume index (22.28 ± 7.85 vs. 18.21 ± 5.14 mL/m^2, $p = 0.003$). Despite preserved 3D EF (70.79 ± 5.98% vs. 72.07 ± 5.76%, $p = 0.276$), global longitudinal strain (GLS) was significantly impaired (−18.56 ± 2.37% vs. −21.47 ± 1.86%, $p < 0.001$). 3D volumetric parameters demonstrated superior diagnostic performance (AUC for LVEDVI Z-score = 0.874) compared to conventional indices. Transfusion duration correlated strongly with ventricular volumes (r = 0.569 for EDV, $p < 0.001$), while serum ferritin showed no significant correlation with cardiac parameters. **Conclusions:** Children with TDßT develop early subclinical LV dysfunction detectable by 3DE and strain analysis despite preserved conventional systolic indices. 3D volumetry and GLS should be integrated into routine cardiac surveillance protocols to enable timely therapeutic intervention.

Keywords: beta-thalassemia; left ventricular function; three-dimensional echocardiography; speckle-tracking echocardiography; iron overload cardiomyopathy

Academic Editor: Paolo Ricchi

Received: 30 April 2026
Revised: 12 June 2026
Accepted: 16 June 2026
Published: 19 June 2026

1. Introduction

Transfusion-dependent beta-thalassemia (TDßT) is the most severe form of this inherited hemoglobinopathy, affecting millions worldwide, particularly in the Mediterranean basin, Middle East, and Southeast Asia [1]. While regular blood transfusions have transformed TDßT from a universally fatal pediatric illness into a manageable chronic condition,

they inevitably lead to progressive iron overload, with cardiac deposition being the primary cause of mortality, accounting for approximately 70% of TDßT-related deaths [2,3].

The pathophysiology of thalassemic cardiomyopathy involves a dual insult: chronic volume overload from anemia-induced high-output state compounded by direct iron-mediated oxidative damage to myocardial cells [4,5]. Iron enters cardiomyocytes primarily through L-type calcium channels, triggering Fenton chemistry that generates reactive oxygen species, leading to mitochondrial dysfunction, lipid peroxidation, and ultimately ferroptosis, a regulated form of cell death distinct from apoptosis [6,7]. This process results in progressive myocardial fibrosis, diastolic dysfunction, and eventually systolic failure [8].

Traditionally, clinical surveillance has relied on two-dimensional echocardiography (2DE) with left ventricular ejection fraction (LVEF) as the primary metric for cardiac function evaluation. However, this approach has significant limitations. The compensatory hyperdynamic state induced by chronic anemia often masks early myocardial injury, maintaining a normal or even supranormal LVEF despite underlying pathology [9,10]. Furthermore, 2DE relies on geometric assumptions that may not accurately reflect true ventricular volumes, particularly when the heart undergoes spherical remodeling, a common adaptation in chronic volume overload states [11].

Advanced echocardiographic techniques offer potential solutions to these limitations. Three-dimensional echocardiography (3DE) provides direct volumetric measurements without geometric assumptions, enabling accurate assessment of ventricular dimensions and ejection fraction [12,13]. Speckle-tracking echocardiography (STE) allows angle-independent assessment of myocardial deformation (strain), a more sensitive marker of intrinsic contractility that can detect subclinical dysfunction before EF declines [14,15]. GLS, in particular, has emerged as a sensitive predictor of adverse outcomes in various cardiomyopathies, including iron overload conditions [10].

Despite these technological advances, comprehensive data on LV function in pediatric TDßT populations remain limited, particularly in resource-limited settings where cardiac magnetic resonance (CMR) with T2* quantification, the current gold standard for myocardial iron assessment, is often unavailable [16]. Moreover, the comparative diagnostic performance of 2D versus 3D techniques in this specific population has not been systematically evaluated.

This study aimed to comprehensively evaluate LV function in children with TDßT using advanced echocardiographic techniques, including 3DE volumetry and strain analysis, and to determine the diagnostic value of these techniques compared to conventional parameters in detecting early myocardial dysfunction.

2. Patients and Methods

2.1. Study Design

The present study was conducted at the Cardiology Unit of Alexandria University Children's Hospital from November 2024 to September 2025. The study was conducted in accordance with the principles of the Declaration of Helsinki. Ethics approval was obtained from the Faculty of Medicine Ethics Committee (IRB number 00012098, approval number 0108731), Alexandria University, Egypt. Written informed ascent/consent was obtained from all patients/legal guardians before the study.

This case–control study enrolled 50 pediatric patients with a confirmed diagnosis of TDßT based on hemoglobin electrophoresis or a beta-globin gene mutation panel. Inclusion criteria comprised a regular transfusion regimen (≥8 packed red blood cell transfusions/year), ongoing iron chelation therapy, and age between 6 and 18 years. Exclusion criteria included structural heart disease (congenital or rheumatic), overt heart failure (New York Heart Association Functional Classification class II–IV), chronic comor-

bidities affecting cardiac function (hypertension, chronic kidney disease, diabetes mellitus, dyslipidemia, obesity, autoimmune diseases), and metabolic causes of heart failure (hypercalcemia, thyrotoxicosis).

The control group consisted of 50 age- and sex-matched healthy children with no clinical or echocardiographic evidence of heart disease. Sample size was determined based on a previous study by Hider et al. [17], with a minimum total required sample size of 100 children (50 per group) to achieve 80% power and detect a difference of 3 mL/m^2 in Left ventricular end-systolic volume index (LVEDVI) between groups, using a two-sided independent sample *t*-test at a significance level of 0.05.

2.2. Clinical, Laboratory and Echocardiographic Assessment

All participants underwent a comprehensive clinical evaluation, including medical history, physical examination, and anthropometric measurements. Weight and height were recorded and converted to Z-scores according to the CDC growth charts [18]. Body surface area (BSA) was calculated using the Mosteller formula: $\sqrt{\text{height in cm} \times \text{weight in kg}/3600}$.

For TDßT patients, medical records were reviewed for disease duration, age at treatment initiation, transfusion regimen, details of chelation therapy, and history of cardiac symptoms (chest pain, palpitations, syncope). Pre-transfusion blood samples were analyzed for complete blood count, liver and renal function tests, while serum ferritin levels were calculated as the mean of available readings over the preceding 12 months.

Echocardiographic examinations were performed by a single experienced operator blinded to participant status using a Philips EPIQ 7C ultrasound system (Philips Medical Systems, Andover, MA, USA) equipped with an X5-1 matrix-array transducer (1–5 MHz). All echocardiographic assessments were performed within one week post-transfusion, but never on the same day of transfusion, to ensure standardization of loading conditions, hemoglobin levels, and volume status across the patient cohort. All participants were examined in the left lateral decubitus position during quiet breathing or a breath hold, as appropriate. Standard 2DE was performed according to current guidelines [19]. Left ventricular end-diastolic volume (LVEDV) and end-systolic volume (LVESV) were measured using the Teichholz method from M-mode parasternal long-axis views and the biplane Simpson's method from apical views. LVEF was calculated using both methods. Fractional shortening (FS) was derived from M-mode measurements. All measurements were averaged over three consecutive cardiac cycles.

Pulsed-wave tissue Doppler imaging (TDI) was performed at the septal and lateral mitral annulus from the apical four-chamber view. The following parameters were measured: systolic myocardial velocity (S′), early diastolic myocardial velocity (E′), and late diastolic myocardial velocity (A′). The myocardial performance index (MPI) was calculated as (isovolumic contraction time + isovolumic relaxation time)/ejection time. 2D STE was performed using offline analysis software (AutoLV from TOMTEC-ARENA TTA2.50.00 Philips QLAB, TOMTEC Imaging Systems GmbH, Unterschleißheim, Germany). Two-chamber, three-chamber, and four-chamber views were acquired with frame rates > 60 frames per second. The software automatically tracked endocardial and epicardial borders frame by frame. GLS was calculated as the average of strain curves from all LV segments. Adequate tracking was verified by visual inspection and software confirmation.

Full-volume 3D datasets were acquired from the apical window using multi-beat mode over 4–6 consecutive cardiac cycles during breath-hold to minimize artifacts. Images were displayed from the 3D volume dataset, and manual adjustments were performed when necessary. The following LV parameters were measured: Left ventricular end-diastolic volume (LVEDV, mL), Left ventricular end-systolic volume (LVESV, mL), Left ventricular end-diastolic volume index (LVEDVI, mL/m^2), Left ventricular end-systolic volume index

(LVESVI, mL/m^2), Left ventricular ejection fraction (3D EF, %), Stroke volume index (SVI, mL/m^2). All 3D parameters were correlated with the Boston Children's Hospital Z-score system for age-appropriate normative values [20].

2.3. Statistical Analysis

Statistical analysis was performed using IBM SPSS Statistics version 27.0 (Armonk, NY, USA: IBM Corp.) and MedCalc Statistical Software v20.0. Continuous variables were expressed as mean ± standard deviation (SD) or median and interquartile range (IQR) based on distribution normality (Shapiro–Wilk test). Categorical variables were presented as numbers and percentages. Between-group comparisons used Student's *t*-test for normally distributed variables and the Mann–Whitney U test for non-normally distributed variables. Categorical variables were compared using the chi-square test. A paired *t*-test was used to compare 2D and 3D measurements within the same group. Correlations were assessed using the Pearson coefficient for normally distributed variables and the Spearman coefficient for non-normally distributed variables. To evaluate the clinical utility of advanced imaging, the diagnostic performance of conventional and 3D parameters was assessed using the Receiver Operating Characteristic (ROC) curve. The Area Under the Curve (AUC) was calculated to determine the overall accuracy of each parameter in discriminating TDßT patients from healthy controls. Optimal diagnostic cut-off values were identified using Youden's index. Two-tailed $p < 0.05$ was considered statistically significant.

3. Results

The demographic characteristics of the 50 included TDßT patients and 50 age- and sex-matched healthy controls were comparable with respect to sex distribution (46.0% male in patients vs. 58.0% in controls, $p = 0.230$) and age (9.73 ± 2.85 vs. 9.54 ± 2.81 years, $p = 0.717$), confirming appropriate matching. TDßT patients exhibited significant growth retardation compared to controls, with lower mean height Z-score (−1.39 ± 0.85 vs. −0.16 ± 1.10, $p < 0.001$) and weight Z-score (−0.55 ± 0.95 vs. −0.14 ± 0.99, $p = 0.039$). Body surface area and BMI Z-scores did not differ significantly between groups, suggesting maintained body proportionality despite linear growth stunting. Vital signs revealed a hyperdynamic state in patients, with significantly higher heart rate (95.30 ± 14.06 vs. 87.48 ± 10.04 bpm, $p = 0.002$).

Patients with TDßT had long-standing disease with a mean transfusion duration of 9.22 ± 2.82 years and chelation therapy duration of 7.98 ± 2.77 years. Mean serum ferritin level was 1395.3 ± 857.3 ng/mL, with 86% of patients having levels <2500 ng/mL, 10% with levels 2500–5000 ng/mL, and 4% with levels >5000 ng/mL. The mean frequency of blood transfusions was 10.88 ± 3.16 per year. Laboratory analysis showed significantly lower mean hemoglobin in patients than in controls (9.85 ± 0.47 vs. 11.25 ± 0.93 g/dL, $p < 0.001$), reflecting chronic anemia despite transfusion support. Liver enzymes were significantly higher in patients compared to controls (ALT: 36.44 ± 10.33 vs. 25.38 ± 8.49 U/L, $p < 0.001$; AST: 55.26 ± 13.02 vs. 29.44 ± 8.39 U/L, $p < 0.001$), indicating iron-related hepatocellular involvement.

3.1. Echocardiographic Parameters

Table 1 shows that the 2D parameters revealed no significant differences in LV volumes between the two groups, except for 2D EF and GLS, which were significantly lower in patients compared to controls, though still within the normal range. Moreover, GLS by 2D STE was significantly reduced in TDßT patients ($p < 0.001$), revealing subclinical myocardial dysfunction despite the preserved EF. On the other hand, TDI demonstrated significant differences in myocardial function between the two groups, with significantly

reduced Septal and lateral S′ velocity in patients compared to controls ($p < 0.001$ and $p = 0.005$, respectively). The myocardial performance index was significantly elevated in patients compared to controls at both septal and lateral walls ($p < 0.001$ for both), indicating combined systolic-diastolic dysfunction.

Table 1. Comparison of conventional echocardiographic parameters between TDßT patients and controls.

Parameter	TDßT Patients (n = 50)	Controls (n = 50)	*p*-Value
2D Parameters			
EDV (mL)	75.08 ± 22.46	77.66 ± 21.78	0.562
EDVI (mL/m^2)	71.97 ± 20.17	72.92 ± 12.01	0.776
ESV (mL)	25.95 ± 9.22	24.00 ± 6.80	0.232
ESVI (mL/m^2)	24.48 ± 7.98	22.38 ± 4.12	0.103
EF (%)	65.31 ± 7.12	69.21 ± 3.87	0.001 *
GLS (%)	−18.56 ± 2.37	−21.47 ± 1.86	<0.001 *
TDI Parameters			
Septal S′ (cm/s)	7.40 ± 1.15	8.79 ± 1.40	<0.001 *
Septal E′ (cm/s)	10.33 ± 2.79	10.77 ± 2.41	0.401
Septal MPI	0.51 ± 0.09	0.36 ± 0.03	<0.001 *
Lateral S′ (cm/s)	8.26 ± 1.11	9.05 ± 1.58	0.005 *
Lateral E′ (cm/s)	13.05 ± 2.57	16.87 ± 3.01	<0.001 *
Lateral MPI	0.52 ± 0.09	0.37 ± 0.03	<0.001 *

Data presented as mean ± SD. * $p < 0.05$ is considered statistically significant. TDßT: Transfusion-dependent beta-thalassemia, 2D: Two-dimensional, EDV: End-diastolic volume, EDVI: End-diastolic volume index, ESV: End-systolic volume, ESVI: End-systolic volume index, EF: Ejection fraction, GLS: Global longitudinal strain, TDI: Tissue Doppler imaging, S′: Peak systolic myocardial velocity, E′: Early diastolic myocardial velocity, MPI: Myocardial performance index, SD: Standard deviation.

3.2. Three-Dimensional Echocardiographic Parameters

In contrast to 2D findings, 3DE revealed significant ventricular dilation in TDßT patients (Table 2). LVEDVI and LVESVI Z-scores were significantly higher in patients compared to controls ($p = 0.002$ and $p = 0.003$, respectively). Despite these volumetric differences, 3D EF did not differ significantly between groups. However, stroke volume index was significantly higher in patients ($p = 0.009$), reflecting the compensatory high-output state.

Table 2. Comparison of 3D echocardiographic parameters between TDßT patients and controls.

Parameter	TDßT Patients (n = 50)	Controls (n = 50)	*p*-Value
EDV (mL)	81.24 ± 27.03	68.83 ± 19.35	0.010 *
EDVI (mL/m^2)	75.50 ± 17.99	65.63 ± 11.86	0.002 *
LVEDVI Z-score	1.53 ± 1.33	0.47 ± 0.97	<0.001 *
ESV (mL)	24.60 ± 11.87	19.00 ± 6.65	0.031 *
ESVI (mL/m^2)	22.28 ± 7.85	18.21 ± 5.14	0.003 *
LVESVI Z-score	−0.19 ± 1.36	−1.02 ± 0.84	<0.001 *
SV (mL)	56.65 ± 16.25	49.86 ± 14.76	0.031 *
SVI (mL/m^2)	53.18 ± 12.22	47.39 ± 9.45	0.009 *
EF (%)	70.79 ± 5.98	72.07 ± 5.76	0.276

Data presented as mean ± SD. * $p < 0.05$ considered statistically significant. 3D: Three-dimensional echocardiography, EDV: End-diastolic volume, EDVI: End-diastolic volume index, LVEDVI: Left ventricular end-diastolic volume index, ESV: End-systolic volume, ESVI: End-systolic volume index, LVESVI: Left ventricular end-systolic volume index. SV: Stroke volume, SVI: Stroke volume index, EF: Ejection fraction, SD: Standard deviation.

3.3. Comparison Between 2D and 3D Measurements

Paired analysis within each group revealed significant discrepancies between 2D and 3D measurements (Table 3). In TDßT patients, 2D underestimated LVEDV compared with 3D (75.08 ± 22.46 vs. 81.24 ± 27.03 mL, $p = 0.158$), though the difference was not statistically significant. More importantly, 2D EF was significantly lower than 3D EF in both patients and controls ($p < 0.001$ and $p = 0.006$, respectively). In controls, 2D significantly overestimated LVEDVI compared to 3D ($p = 0.002$), while in patients, the difference was less pronounced ($p = 0.376$).

Table 3. Comparison between 2D and 3D measurements within each group.

Parameter	TDßT Patients (n = 50)			Controls (n = 50)		
	2D	3D	*p*-Value	2D	3D	*p*-Value
EDV (mL)	75.08 ± 22.46	81.24 ± 27.03	0.158	77.66 ± 21.78	68.83 ± 19.35	<0.001 *
EDVI (mL/m^2)	71.97 ± 20.17	75.50 ± 17.99	0.376	72.92 ± 12.01	65.63 ± 11.86	0.002 *
ESV (mL)	25.95 ± 9.22	24.60 ± 11.87	0.412	24.00 ± 6.80	19.00 ± 6.65	<0.001 *
ESVI (mL/m^2)	24.48 ± 7.98	22.28 ± 7.85	0.164	22.38 ± 4.12	18.21 ± 5.14	<0.001 *
EF (%)	65.31 ± 7.12	70.79 ± 5.98	<0.001 *	69.21 ± 3.87	72.07 ± 5.76	0.006 *

Data presented as mean ± SD. * $p < 0.05$ is considered statistically significant. 2D: Two-dimensional, 3D: Three-dimensional, EDV: End-diastolic volume, EDVI: End-diastolic volume index, ESV: End-systolic volume, ESVI: End-systolic volume index, EF: Ejection fraction, SD: Standard deviation.

3.4. Correlations with Disease Parameters

The duration of blood transfusion showed significant positive correlations with all 3D LV volumes except LVEDVI which showed no correlation and a significant negative correlation with 3D EF. Transfusion frequency also correlated significantly with both LVEDVI and LVESVI. In contrast, serum ferritin levels showed no significant correlation with any 3D volumetric or functional parameters (Table 4).

Table 4. Correlation between disease parameters and 3D LV parameters in TDßT patients.

Parameter	Duration of Transfusion		Ferritin (ng/mL)		Transfusion Frequency/Year	
	r	*p*	r	*p*	r	*p*
EDV (mL)	0.569	<0.001 *	0.194	0.176	-	-
EDVI (mL/m^2)	0.012	0.993	0.027	0.853	0.300	0.034 *
ESV (mL)	0.624	<0.001 *	0.181	0.208	-	-
ESVI (mL/m^2)	0.305	0.031 *	0.084	0.560	0.376	0.007 *
EF (%)	−0.521	<0.001 *	−0.088	0.544	-	-

r: Pearson or Spearman correlation coefficient. * $p < 0.05$ is considered statistically significant. EDV: End-diastolic volume, EDVI: End-diastolic volume index, ESV: End-systolic volume, ESVI: End-systolic volume index, EF: Ejection fraction.

3.5. Diagnostic Performance of Echocardiographic Parameters

By ROC curve analysis, the diagnostic performance of 3D parameters was superior compared to conventional indices (Table 5). LVEDVI Z-score achieved an AUC of 0.874 (95% CI: 0.794–0.954, $p < 0.001$) and LVESVI Z-score showed an AUC of 0.764 (95% CI: 0.657–0.871, $p < 0.001$). 2D EF demonstrated modest diagnostic accuracy (AUC = 0.674, 95% CI: 0.562–0.786, $p = 0.004$), while TAPSE showed poor discriminatory ability (AUC = 0.572, $p = 0.252$). Also, Figure 1 showed that there is a notable discrepancy between 2D and 3D EDVI as 2D measurement failed to predict the condition (AUC = 0.500, $p = 0.997$). In contrast, 3D EDVI was a significant predictor (AUC = 0.676, $p = 0.002$). In addition, Average GLS emerged as a high-performing parameter as it yielded an AUC of 0.838 ($p < 0.001$) with a cut-off of −19.6; it provided a balanced prognostic profile with 72% sensitivity and 80% specificity, as shown in Figure 2.

Table 5. Diagnostic performance of echocardiographic parameters for discriminating TDßT patients from controls.

Parameter	AUC (95% CI)	*p*-Value	Cut-Off	Sensitivity (%)	Specificity (%)
Conventional Parameters					
2DE EF (%)	0.674 (0.562–0.786)	0.004 *	≤68.7%	68.0	64.0
TAPSE (mm)	0.572 (0.453–0.692)	0.252	≤20.6	56.0	60.0
3DE Volumetric Parameters					
LVEDVI Z-score	0.874 (0.794–0.954)	<0.001 *	>0.85	74.0	90.0
LVESVI Z-score	0.764 (0.657–0.871)	<0.001 *	>−0.65	68.0	84.0
Strain Parameters					
GLS (%)	0.824 (0.727–0.922)	<0.001 *	≤−19.5%	78.0	82.0

* $p < 0.05$ is considered statistically significant. AUC: Area under the curve, CI: Confidence interval, EF: Ejection fraction, TAPSE: Tricuspid annular plane systolic excursion, 3DE: Three-dimensional echocardiography, LVEDVI: Left ventricular end-diastolic volume index, LVESVI: Left ventricular end-systolic volume index, GLS: Global longitudinal strain.

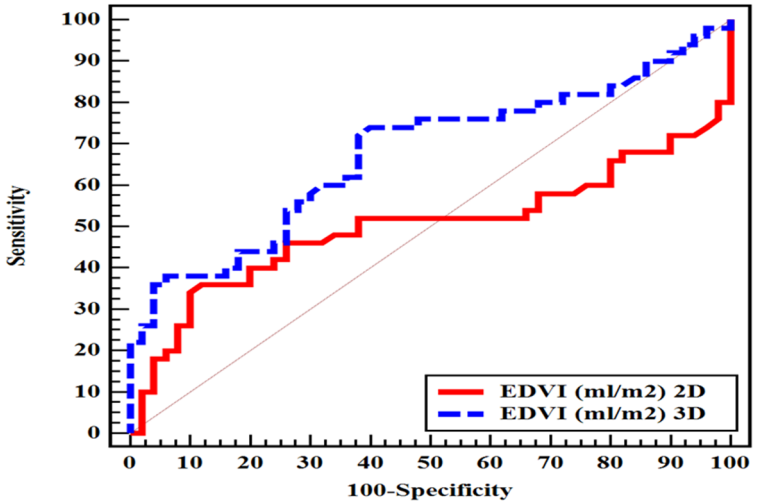

Figure 1. ROC curve for EDVI 2D and 3D to predict children with β-TDT from healthy individuals.

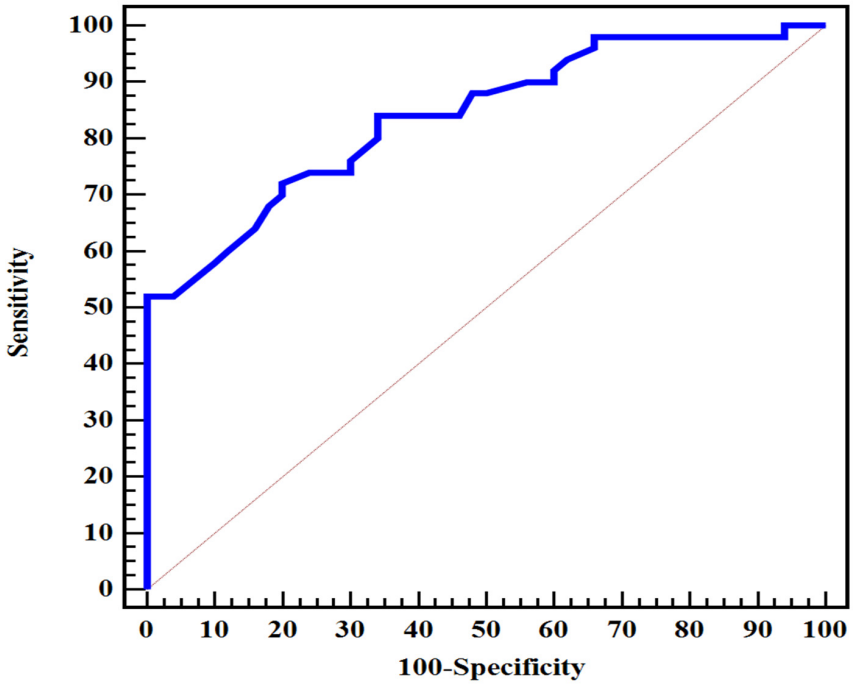

Figure 2. ROC curve for Average GLS to predict children with β-TDT from healthy individuals.

4. Discussion

In the present case–control study of children with TDßT, we identified a distinct LV phenotype characterized by apparent preservation of global pump function on conventional assessment yet significant impairment of intrinsic myocardial mechanics and occult ventricular dilation detectable only with advanced 3DE techniques. Crucially, because all echocardiographic examinations were systematically standardized and performed within one week post-transfusion, these findings carry heightened clinical weight. By evaluating these pediatric patients at a point in their cycle when hemoglobin levels are optimized and acute anemic volume fluctuations have stabilized, the documented ventricular alterations cannot be dismissed as temporary pre-transfusion volume stretching. Instead, they unmask a state of permanent, chronic structural remodeling that conventional 2D imaging entirely misses.

The most striking finding of this study is the discordance between preserved or enhanced global systolic indices and underlying myocardial dysfunction. TDßT patients demonstrated significantly higher stroke volume index and 3D EF within the normal range, consistent with the physiological consequences of chronic anemia and high-output circulation described by Taher et al. [1] and Kremastinos et al. [2]. Increased preload from expanded blood volume, reduced afterload from peripheral vasodilation, and neurohumoral activation all contribute to augmented global systolic performance.

However, this hyperdynamic state masks progressive myocardial injury. The significant reduction in GLS in patients compared to controls, despite preserved 3D EF, represents the hallmark of early cardiomyopathy. The differential vulnerability of myocardial fiber layers mechanistically explains this dissociation. Longitudinal fibers concentrated in the subendocardium are particularly susceptible to ischemia, mechanical stress, and iron toxicity due to their location and metabolic demands [21]. As iron accumulates and wall tension increases from ventricular dilation, these fibers fail first, reducing longitudinal deformation while radial and circumferential fibers maintain global pump function [22].

Our findings align with the growing body of literature establishing GLS as a sensitive prognostic marker. A recent meta-analysis by Attar et al. [10] proposed a GLS threshold of −19.5% for detecting myocardial iron overload, and our cohort's mean GLS of −18.56% clearly falls within the pathological range. Eroğlu et al. [22] similarly demonstrated GLS reductions in asymptomatic TDßT children (mean −16.8% vs. −18.8% in controls) despite preserved EF.

A striking finding of this study is the diagnostic failure of conventional 2D echocardiography to accurately quantify left ventricular volumes in this patient population. While 2D echocardiography significantly overestimated LVEDVI in healthy controls compared to 3D ($p = 0.002$), it completely failed to predict thalassemic modifications in the patient cohort, yielding a flat, non-discriminatory area under the curve (2D EDVI AUC = 0.500, $p = 0.997$). In stark contrast, 3D volumetric indexing successfully exposed significant ventricular dilation in the TDßT group ($p = 0.002$), proving to be a highly significant diagnostic predictor (3D EDVI AUC = 0.676, $p = 0.002$). This diagnostic blind spot in conventional imaging stems from two primary technical and anatomical limitations. First, standard 2D echocardiography relies on rigid, predefined geometric assumptions, most notably the prolate ellipse model, which presumes a uniform, symmetrical ventricular architecture [11].

However, the chronic volume overload state inherent to TDßT forces an eccentric hypertrophic response, resulting in spherical remodeling that transforms the left ventricle into a more globular configuration to mitigate wall stress. This morphologic distortion invalidates the geometric formulas underlying 2D calculation algorithms, introducing systematic underestimation errors in diseased hearts [23]. Second, because 2D imaging captures only a single slice plane, it is highly vulnerable to apical foreshortening, as the scanning plane

frequently cuts off-axis and excludes the true apical cap [24]. 3DE entirely circumvents these limitations by acquiring a real-time, pyramid-shaped full volumetric dataset, allowing direct geometric calculation of the endocardial border without mathematical modeling [13].

The clinical implications are substantial. If interpreted in isolation, the 2D data from our study might falsely reassure clinicians that thalassemic hearts have not undergone significant dilation. This oversight could be dangerous, leading to delays in escalating chelation or heart failure therapy. The 3D data showing significant ventricular dilation underscore the need for 3D volumetry for accurate risk stratification. To clearly delineate these technological differences and their clinical impact in thalassemic surveillance, a comprehensive structural and performance comparison is outlined in Table 6.

Table 6. Architectural and Performance Comparison: 2D vs. Advanced 3D/Strain Techniques in TDßT Surveillance.

Diagnostic Domain	Conventional 2D Echocardiography	Advanced 3DE & Speckle-Tracking	Clinical & Pathophysiological Implication in TDßT
Geometric Modeling	Relies on geometric assumptions (prolate ellipse model).	Pure volumetric acquisition without structural assumptions.	2D fails to account for the spherical remodeling and eccentric hypertrophy caused by thalassemic chronic volume overload.
Imaging Planes	Prone to apical foreshortening and off-axis slice cuts.	Captures the entire ventricular volume pyramid simultaneously.	3D eliminates systematic underestimation of volumes, capturing early pathological dilation.
Detection of Dilation	Failed to find significant differences in EDVI or ESVI between groups ($p > 0.05$).	Revealed highly significant ventricular dilation ($p = 0.002$ for LVEDVI).	Relying on 2D indices falsely reassures clinicians, potentially delaying vital escalation of iron chelation therapy.
Diagnostic Accuracy (ROC Analysis)	Modest to poor accuracy (2D EDVI AUC = 0.500; 2D EF AUC = 0.674).	Superior diagnostic accuracy (LVEDVI Z-score AUC = 0.874; GLS AUC = 0.824).	3D parameters provide accurate risk stratification tools, especially in resource-limited clinics lacking CMR T2*.
Subclinical Myocardial Injury	Preserved/hyperdynamic EF masks early tissue deterioration.	GLS captures precise longitudinal mechanical strain failure.	Longitudinal subendocardial fibers fail early due to iron toxicity and wall tension before radial fibers drop global EF pump function.

Moreover, ROC curve analysis confirmed the superior diagnostic performance of 3D parameters. LVEDVI Z-score achieved an AUC of 0.874, substantially exceeding that of 2D EF (AUC = 0.674) and conventional TDI indices. This finding has important practical implications. In resource-limited settings where CMR T2* is unavailable, 3DE and strain analysis provide a viable alternative for identifying patients at risk of cardiomyopathy. The optimal cut-off for LVEDVI Z-score (>0.85) provided 74% sensitivity and 90% specificity, enabling accurate identification of pathological dilation. Similarly, the GLS cut-off of −19.5% aligns with previously proposed thresholds, offering a practical screening tool for subclinical dysfunction [10].

A critical negative finding in the present study is the absence of significant correlation between serum ferritin levels and any 3D functional or volumetric parameter. This observation aligns with the literature, which demonstrates that serum ferritin poorly reflects myocardial iron burden [25]. Multiple mechanisms explain this disconnect; first, iron uptake and clearance kinetics differ substantially between organs. Cardiac tissue accumulates and clears iron at a slower rate than hepatic tissue, creating a deceptive clinical picture where a patient may achieve hepatic chelation success with low serum ferritin yet still harbor significant myocardial iron deposits [26,27]. Second, ferritin functions as an acute-phase reactant, susceptible to fluctuations from concurrent inflammation, infection, or hepatic injury [28]. Third, the myocardial iron entry pathway via L-type calcium channels operates independently of systemic iron indices, with uptake determined primarily by circulating labile plasma iron concentration rather than total body stores [7]. This finding has profound clinical implications: a "safe" ferritin level (<2500 ng/mL, observed in 86% of our cohort) does not guarantee cardiac safety. Direct myocardial assessment remains mandatory.

In contrast to ferritin, transfusion duration emerged as the strongest predictor of cardiac remodeling. The significant correlations with LVEDV (r = 0.569), LVESV (r = 0.624), and 3D LVEF (r = −0.521) support the concept that cumulative exposure to iron and hemodynamic stress drives progressive myocardial injury. This finding aligns with the pathophysiological understanding that iron-mediated damage is time-dependent. Each transfusion contributes to the cumulative iron burden, and each year of disease adds to the hemodynamic stress on the ventricle. The significant correlation between transfusion frequency and volumetric indices (LVEDVI: r = 0.300, $p = 0.034$; LVESVI: r = 0.376, $p = 0.007$) further supports this cumulative exposure model. These results suggest that older children with longer transfusion histories represent the highest-risk subgroup, irrespective of current ferritin levels. This emphasizes the importance of early initiation of effective chelation and the need for intensified surveillance as disease duration increases.

TDI findings further supported the strain data independently. Reduced S′ velocities at both septal and lateral annuli confirm impaired longitudinal systolic contraction. The significantly elevated MPI in patients indicates global cardiac inefficiency, with the heart spending disproportionate time in non-ejecting phases, a consequence of delayed relaxation and sluggish contraction onset. These findings align with those of Ibrahim et al. [29], who reported higher MPI in TDßT children and proposed MPI as an early marker of myocardial dysfunction. Importantly, MPI effectively penetrates the compensatory hemodynamic effects that mask EF decline, revealing underlying tissue rigidity and electromechanical conduction delays from chronic iron deposition.

5. Conclusions

Children with TDßT exhibit early, subclinical left ventricular dysfunction detectable by 3D echocardiography and speckle-tracking strain analysis, despite preserved conventional systolic indices. Three-dimensional volumetry reveals significant ventricular dilation missed by conventional 2D imaging, while GLS identifies intrinsic myocardial mechanical failure preceding ejection fraction decline. The duration of transfusion therapy, rather than serum ferritin levels, emerges as the primary predictor of cardiac remodeling, emphasizing cumulative exposure as the key risk factor. The diagnostic superiority of 3D parameters over conventional indices supports their integration into routine cardiac surveillance protocols. Early detection of subclinical dysfunction may enable timely therapeutic intervention, including optimization of chelation therapy, potentially altering the natural history of thalassemic cardiomyopathy, which remains the leading cause of mortality in this vulnerable population. In resource-limited settings where CMR is unavailable, 3D echocardiography and strain analysis provide essential tools for risk stratification and clinical decision-making.

5.1. Clinical Implications

The findings of this study carry several important clinical implications. First, current surveillance protocols, which rely primarily on 2D EF and ferritin levels, are insufficient. In our cohort, 86% of patients had ferritin levels <2500 ng/mL, yet 3D revealed significant ventricular dilation and strain impairment. This suggests widespread undetected cardiac involvement that may progress without intervention. Second, 3D volumetry should replace or supplement 2D methods for routine surveillance in thalassemia centers. The ability to accurately track ventricular volumes enables early detection of pathological dilation and provides objective metrics for assessing disease progression. Third, GLS should be integrated into routine protocols. A decline in GLS, even with normal EF, should trigger clinical review of chelation efficacy and consideration for cardiac-specific chelators (deferiprone or combination therapy) known to reduce myocardial iron burden [30,31]. Finally, risk

stratification should adopt a multi-parametric approach combining 3D volumetry, GLS, and, when available, CMR T2* imaging, rather than relying solely on biochemical markers.

Nevertheless, several limitations of the present study should be acknowledged. First, the absence of CMR T2* assessment, the current clinical gold standard, prevented direct validation of our advanced strain and volumetric abnormalities against actual myocardial iron concentrations. Consequently, it remains highly challenging to definitively isolate whether the observed early subclinical dysfunction is purely driven by direct intracellular iron overload toxicity or by the chronic, compounding hemodynamic stress of anemia-associated volume overload. The cross-sectional design precludes prognostic inference regarding the trajectory from subclinical dysfunction to overt cardiomyopathy. The single-center design and modest sample size may limit generalizability, though the sample was adequately powered for primary outcomes. The technical demands of advanced echocardiography may limit widespread adoption, though automated analysis software is increasingly available. Additionally, the impact of different iron chelation regimens, compliance levels, and transfusion adequacy on LV function was not analyzed.

5.2. Future Directions

Longitudinal studies integrating serial 3DE and CMR T2* measurements are needed to establish the natural history of subclinical dysfunction and define thresholds for intervention. The prognostic value of 3D volumetric and strain parameters should be evaluated against clinical outcomes, including heart failure development and mortality. Additionally, the role of 3D techniques in guiding the intensification of chelation therapy requires prospective evaluation. Could GLS decline serve as a trigger for switching to more aggressive chelation regimens? Could normalization of strain after intensified therapy predict favorable outcomes? These questions warrant investigation.

Author Contributions: All authors contributed to the study conception and design. A.S.A., O.R. and H.M.A. performed material preparation, data collection, and analysis. O.R. conducted the echocardiographic examination. H.M.A. revised the echocardiographic images. O.R., A.S.A., H.M.A. and Y.E.C. contributed to the interpretation of results. A.S.A. and O.R. wrote the first draft of the manuscript. All authors have read and agreed to the published version of the manuscript.

Funding: This research received no funding.

Institutional Review Board Statement: The study was conducted in accordance with the principles of the Declaration of Helsinki. Ethics approval was obtained from the Faculty of Medicine Ethics Committee (IRB number 00012098, approval number 0108731), Alexandria University, Egypt.

Informed Consent Statement: Written informed ascent/consent was obtained from all patients/legal guardians before the study.

Data Availability Statement: De-identified data are available from the corresponding author upon reasonable request for privacy.

Acknowledgments: We thank patients and their families for participating in the study and the staff of the Hematology clinic at Alexandria University Children's Hospital for their cooperation.

Conflicts of Interest: The authors have no relevant financial or non-financial interests to disclose.

Abbreviations

2D	Two-dimensional
2DE	Two-dimensional echocardiography
3D	Three-dimensional
3DE	Three-dimensional echocardiography

ALT	Alanine aminotransferase
AST	Aspartate aminotransferase
AUC	Area under the curve
BMI	Body mass index
BSA	Body surface area
CDC	Centers for Disease Control and Prevention
CI	Confidence interval
CMR	Cardiac magnetic resonance
EDV	End-diastolic volume
EDVI	End-diastolic volume index
EF	Ejection fraction
ESV	End-systolic volume
ESVI	End-systolic volume index
FS	Fractional shortening
GLS	Global longitudinal strain
IQR	Interquartile range
LV	Left ventricle/Left ventricular
LVEDV	Left ventricular end-diastolic volume
LVEDVI	Left ventricular end-diastolic volume index
LVEF	Left ventricular ejection fraction
LVESV	Left ventricular end-systolic volume
LVESVI	Left ventricular end-systolic volume index
MPI	Myocardial performance index
ROC	Receiver operating characteristic
SD	Standard deviation
STE	Speckle-tracking echocardiography
SV	Stroke volume
SVI	Stroke volume index
TAPSE	Tricuspid annular plane systolic excursion
TDßT	Transfusion-dependent beta-thalassemia
TDI	Tissue Doppler imaging

References

1. Taher, A.T.; Weatherall, D.J.; Cappellini, M.D. Thalassaemia. *Lancet* **2018**, *391*, 155–167. [CrossRef] [PubMed]
2. Kremastinos, D.T.; Farmakis, D. Iron overload cardiomyopathy in clinical practice. *Circulation* **2011**, *124*, 2253–2263. [CrossRef] [PubMed]
3. Borgna-Pignatti, C.; Rugolotto, S.; De Stefano, P. Survival and complications in patients with thalassemia major treated with transfusion and deferoxamine. *Haematologica* **2004**, *89*, 1187–1193. [PubMed]
4. Origa, R. beta-Thalassemia. *Genet. Med.* **2017**, *19*, 609–619. [PubMed]
5. Rivella, S. beta-thalassemias: Paradigmatic diseases for scientific discoveries and development of innovative therapies. *Haematologica* **2015**, *100*, 418–430. [PubMed]
6. Oudit, G.Y.; Trivieri, M.G.; Khaper, N. Role of L-type Ca2+ channels in iron transport and iron-overload cardiomyopathy. *J. Mol. Med.* **2006**, *84*, 349–364. [PubMed]
7. Fang, X.; Wang, H.; Han, D. Ferroptosis as a target for protection against cardiomyopathy. *Proc. Natl. Acad. Sci. USA* **2019**, *116*, 2672–2680. [CrossRef] [PubMed]
8. Pennell, D.J.; Udelson, J.E.; Arai, A.E. Cardiovascular function and treatment in beta-thalassemia major: A consensus statement from the American Heart Association. *Circulation* **2013**, *128*, 281–308. [CrossRef] [PubMed]
9. Bay, A.; Baspinar, O.; Leblebisatan, G. Detection of left ventricular regional function in asymptomatic children with beta-thalassemia major by longitudinal strain and strain rate imaging. *Turk. J. Hematol.* **2013**, *30*, 283–289. [CrossRef]
10. Attar, A.; Hosseinpour, A.; Hosseinpour, H. Global longitudinal strain for detection of cardiac iron overload in patients with thalassemia: A meta-analysis of observational studies with individual-level participant data. *Cardiovasc. Ultrasound* **2022**, *20*, 13.
11. Lang, R.M.; Badano, L.P.; Mor-Avi, V. Recommendations for cardiac chamber quantification by echocardiography in adults: An update from the American Society of Echocardiography and the European Association of Cardiovascular Imaging. *Eur. Heart J. Cardiovasc. Imaging* **2015**, *16*, 233–270. [CrossRef] [PubMed]

12. Hur, D.J.; Sugeng, L. Integration of three-dimensional echocardiography into the modern-day echo laboratory. *Echocardiography* **2020**, *37*, 2136–2144.
13. Medvedofsky, D.; Maffessanti, F.; Weinert, L. 2D and 3D echocardiography-derived indices of left ventricular function and shape. *JACC Cardiovasc. Imaging* **2018**, *11*, 1569–1579. [CrossRef] [PubMed]
14. Smiseth, O.A.; Torp, H.; Opdahl, A. Myocardial strain imaging: How useful is it in clinical decision making? *Eur. Heart J.* **2016**, *37*, 1196–1207. [PubMed]
15. Muntean, I.; Hack, B.J.; Hagau, A.C. Global longitudinal strain as a sensitive marker of left ventricular dysfunction in pediatric dilated cardiomyopathy: A case-control study. *J. Cardiovasc. Dev. Dis.* **2025**, *12*, 15.
16. Kirk, P.; Roughton, M.; Porter, J.B. Cardiac T2* magnetic resonance for prediction of cardiac complications in thalassemia major. *Circulation* **2009**, *120*, 1961–1968. [CrossRef] [PubMed]
17. Hider, R.C.; Hoffbrand, A.V. The role of deferiprone in iron chelation. *N. Engl. J. Med.* **2018**, *379*, 2140–2150. [CrossRef] [PubMed]
18. Kuczmarski, R.J.; Ogden, C.L.; Guo, S.S.; Grummer-Strawn, L.M.; Flegal, K.M.; Mei, Z.; Wei, R.; Curtin, L.R.; Roche, A.F.; Johnson, C.L. *2000 CDC Growth Charts for the United States: Methods and Development*; Vital and Health Statistics: Series 11; National Health Survey: Hyattsville, MD, USA, 2002; Volume 246, pp. 1–190.
19. Lopez, L.; Saurers, D.L.; Barker, P.C.; Cohen, M.S.; Colan, S.D.; Dwyer, J.; Forsha, D.; Friedberg, M.K.; Lai, W.W.; Printz, B.F.; et al. Guidelines for Performing a Comprehensive Pediatric Transthoracic Echocardiogram: Recommendations from the American Society of Echocardiography. *J. Am. Soc. Echocardiogr.* **2024**, *37*, 119–183. [CrossRef] [PubMed]
20. Boston Children's Hospital. Z-Score Calculator. Available online: https://zscore.chboston.org/ (accessed on 30 November 2025).
21. Anderson, P.G.; Bishop, S.P.; Peterson, J.T. *Cardiovascular Research*; Elsevier: Amsterdam, The Netherlands, 2006; pp. 773–802.
22. Eroglu, A.G.; Ulug, N.; Karakas, H. Evaluation of left ventricular function and myocardial deformation in children with beta-thalassemia major by real-time three-dimensional (four-dimensional) and speckle tracking echocardiography. *Echocardiography* **2022**, *39*, 1307–1315. [PubMed]
23. Badano, L.P.; Kolias, T.J.; Muraru, D. Standardization of left atrial, right ventricular, and right atrial deformation imaging using two-dimensional speckle tracking echocardiography. *Eur. Heart J. Cardiovasc. Imaging* **2018**, *19*, 591–600. [CrossRef] [PubMed]
24. Anderson, L.J.; Holden, S.; Davis, B. Cardiovascular T2-star (T2*) magnetic resonance for the early diagnosis of myocardial iron overload. *Eur. Heart J.* **2001**, *22*, 2171–2179. [CrossRef] [PubMed]
25. Coffey, R.; Knutson, M.D. The plasma membrane metal-ion transporter ZIP14 contributes to nontransferrin-bound iron uptake by human beta-cells. *Am. J. Physiol. Cell Physiol.* **2016**, *312*, C169–C175. [PubMed]
26. Nam, H.; Wang, C.Y.; Zhang, L. ZIP14 and DMT1 in the liver, pancreas, and heart are differentially regulated by iron deficiency and overload: Implications for tissue iron uptake in iron-related disorders. *Haematologica* **2013**, *98*, 1049–1057. [CrossRef] [PubMed]
27. Wood, J.C. Estimating tissue iron burden: Current status and future prospects. *Br. J. Haematol.* **2015**, *170*, 15–28. [CrossRef] [PubMed]
28. Sandnes, M.; Ulvik, R.J.; Vorland, M.; Reikvam, H. Hyperferritinemia-a clinical overview. *J. Clin. Med.* **2021**, *10*, 2008. [PubMed]
29. Ibrahim, M.H.; Azab, A.A.; Kamal, N.M. Early detection of myocardial dysfunction in poorly treated pediatric thalassemia children and adolescents: Two Saudi centers experience. *Ann. Med. Surg.* **2016**, *9*, 6–11. [CrossRef]
30. Pepe, A.; Meloni, A.; Rossi, G. Cardiac and hepatic iron and ejection fraction in thalassemia major: Multicentre prospective comparison of combined deferiprone and deferoxamine therapy against deferiprone or deferoxamine monotherapy. *J. Cardiovasc. Magn. Reson.* **2013**, *15*, 1. [CrossRef] [PubMed]
31. Tanner, M.A.; Galanello, R.; Dessi, C. A randomized placebo-controlled double-blind trial of the effect of combined therapy with deferoxamine and deferiprone on myocardial iron in thalassemia major using cardiovascular magnetic resonance. *Circulation* **2007**, *115*, 1876–1884. [CrossRef] [PubMed]